Research Square

Preprints are preliminary reports that have not undergone peer review.
They should not be considered conclusive, used to inform clinical practice,
or referenced by the media as validated information.

Background Liver Fibrosis on Gadoxetate-Enhanced T1 Mapping versus DWI-Based Virtual MR Elastography: A FIB-4-Referenced Comparison

Bo Wang

wangbo871@sina.com

First People's Hospital of Yunnan Province

Weijun Xia

Menghai County People's Hospital

Li Wu

First People's Hospital of Yunnan Province

Jing Yang

First People's Hospital of Yunnan Province

Changyuan Xin

First People's Hospital of Yunnan Province

Research Article

Keywords: Focal Liver Lesion, Liver Fibrosis, Virtual Magnetic Resonance Elastography, T1 Mapping, Indocyanine Green, FIB-4

Posted Date: November 12th, 2026

DOI: https://doi.org/10.21203/rs.3.rs-11449416/v1

License: This work is licensed under a Creative Commons Attribution 4.0 International License.
Read Full License

Additional Declarations: No competing interests reported.

Background Liver Fibrosis on Gadoxetate-Enhanced T1 Mapping versus DWI-Based Virtual MR Elastography: A FIB-4-Referenced Comparison

Bo Wang[1]*, Weijun Xia[2], Li Wu[1]*, Jing Yang[1], Changyuan Xin[1]

1 The First People's Hospital of Yunnan Province, Kunming, China

2 Menghai County People's Hospital, Xishuangbanna, China

* Joint Corresponding authors:

Bo Wang , E-mail: wangbo871@sina.com

Li Wu , E-mail: wuli211@163.com

ABSTRACT

Objective: To evaluate the degree of fibrosis and its correlation with FIB-4 risk stratification in patients with focal liver lesions (FLL) using virtual magnetic resonance elastography (vMRE), T1 mapping before and after gadoxetate disodium (Gd-EOB-DTPA) enhanced imaging, and indocyanine green retention at 15 minutes (ICG-R15).

Method: A total of 86 FLL patients who underwent Gd-EOB-DTPA-enhanced MRI and ICG clearance test within one week were retrospectively enrolled. Based on FIB-4 scores, participants were divided into low-risk group (n=11), moderate-risk group (n=30), and high-risk group (n=45). vMRE stiffness was derived from multi-b-value DWI images at b=200 and 1500 s/mm². Pre-contrast T1 mapping (T1-pre) and 20-min post-contrast T1 mapping (T1-20min), along with T1 relaxation time change rate (ΔT1%), were acquired via modified Look-Locker inversion recovery (MOLLI). Group comparisons used analysis of variance (ANOVA) or Kruskal-Wallis; correlations with FIB-4 used Spearman; diagnostic performance for high-risk used receiver operating characteristic (ROC); independent factors for vMRE used multiple regression.

Result: vMRE, T1-pre, T1-20min, ΔT1%, and ICG-R15 showed significant difference across FIB-4 risk strate. vMRE differed across all pairwise groups (Bonferroni P<0.001). T1-pre differed only between intermediate- and high-risk groups (P<0.001). T1-20min, ΔT1%, and ICG-R15 differed between low- vs high-risk and intermediate- vs high-risk (P<0.001), but not between low- vs intermediate-risk. vMRE correlated positively with FIB-4 (ρ=0.49, P<0.001); ICG-R15 correlated positively with T1-20min (ρ=0.70) and ΔT1% (ρ=0.69) (P<0.001). vMRE showed the highest AUC for high-risk (0.823, 95% CI: 0.735-0.912, sensitivity 68.9%, specificity 87.8%). Multiple regression showed vMRE independently associated with FIB-4 (B=0.088, P<0.001), and was 0.417 kPa lower in females than males (P=0.023), but not with age (P=0.290).

Conclusion: vMRE differed across all FIB-4 strata, whereas gadoxetate-enhanced T1 parameters differed only in some strata, suggesting complementary pathological information. Combined vMRE and ΔT1% may provide structural and functional assessment, requiring further validation.

Keywords: Focal Liver Lesion; Liver Fibrosis; Virtual Magnetic Resonance Elastography; T1 Mapping; Indocyanine Green; FIB-4

1. INTRODUCTION

As the role of imaging in diagnosis and management has grown, the detection rate of asymptomatic incidental liver lesions has increased [1]. Whether the background liver is fibrotic directly affects treatment decisions, including the extent of surgical resection, the risk of ablation, and long-term prognosis [2]. Accurate assessment of fibrosis helps prevent postoperative hepatic decompensation and also has value for predicting tumor recurrence. Evidence shows early recurrence is related to tumor factors, while late recurrence is associated with underlying liver disease [3]. Although liver biopsy

remains the gold standard, its invasiveness, sampling errors, and bleeding risk make it impractical for routine screening in FLL patients, necessitating non-invasive alternatives.

FIB-4, as a non-invasive biomarker, may replace biopsy for fibrosis risk stratification [4]. To date, few studies have specifically focused on FLL patients and simultaneously compared T1-pre, vMRE, ΔT1%, and ICG-R15 with FIB-4 stratification, and direct evidence comparing their diagnostic performance is lacking. Therefore, we performed this retrospective analysis to evaluate these parameters across FIB-4 risk groups and explore factors independently associated with vMRE, aiming to provide imaging references for preoperative background liver assessment in FLL patients.

2. MATERIALS AND METHODS

2.1 Patients

This retrospective study enrolled FLL patients who underwent Gd-EOB-DTPA-enhanced liver MRI (T1 mapping, multi-b-value DWI), serological tests, and ICG clearance at the First People's Hospital of Yunnan Province from Nov 2017 to Apr 2022. The requirement for informed consent was waived due to the retrospective design. Inclusion criteria were: (1) availability of T1 mapping and multi-b-value DWI images from Gd-EOB-DTPA-enhanced MRI; (2) performance of ICG clearance test within one week of the MRI; and (3) completion of complete blood count, liver function, and coagulation tests within the same week. Exclusion criteria were: (1) acute hepatitis or acute exacerbation of chronic hepatitis (ALT >5 times the upper limit of normal); (2) diffuse hepatic malignancy or other diffuse lesions precluding ROI delineation; (3) MRI evidence of severe fatty degeneration; (4) massive ascites or hepatic encephalopathy grade ≥II; (5) significant image artifacts precluding post-processing; and (6) incomplete clinical characteristics or laboratory data. Ultimately, 86 patients were enrolled.

2.2 MRI protocol

MRI was performed on a 1.5T Siemens Area scanner with a 16-channel coil. T1 mapping using the MOLLI sequence was acquired before and 20 minutes post-contrast (single breath-hold, axial slice near the hepatic hilum). Scan parameters were: TR/TE 370/1.0 ms, TI 275 ms, FOV 340×290 mm, matrix 124×192, thickness 8 mm, NEX 1, flip angle 35°. Gd-EOB-DTPA (0.025 mmol/kg at 1.0 mL/s) was injected, followed by 20 mL saline flush at same rate. Multi-b-value DWI (axial) parameters: TR/TE 5400/68 ms, FOV 256×296 mm, matrix 256×256, thickness 5 mm, gap 1 mm, NEX 2, b-values 0–1500 s/mm² (0,50,100,150,200,300,500,800,1000,1200,1500).

2.3 Imaging Analysis

Inter-observer and intra-observer reproducibility were assessed in 20 randomly selected participants. ROIs for vMRE and T1 mapping were measured twice by the same observer and once by a blinded observer. The intra-observer ICC for T1-pre, T1-20min, and vMRE was 0.963, 0.991, and 0.858; the inter-observer ICC was 0.988, 0.996, and 0.907, respectively.

2.4 T1 Mapping Post-processing

T1-pre and T1-20min images were imported into ITK-SNAP (v. 3.8.0). On T1-pre images, circular ROIs (≈2.0 cm² each) were manually placed in the left medial, left lateral, right anterior, and right posterior liver segments, avoiding visible intrahepatic vessels and focal lesions (Figure 1a), and then copied to the corresponding locations on T1-20min images (Figure 1b). Mean T1 relaxation time was calculated from the four ROIs on each image to obtain T1-pre and T1-20min values. ΔT1% was calculated as: (T1-20min − T1-pre) / T1-pre × 100%. Because Gd-EOB-DTPA uptake shortens T1 relaxation time, ΔT1% values are negative, with more negative values indicating greater hepatocyte

uptake.

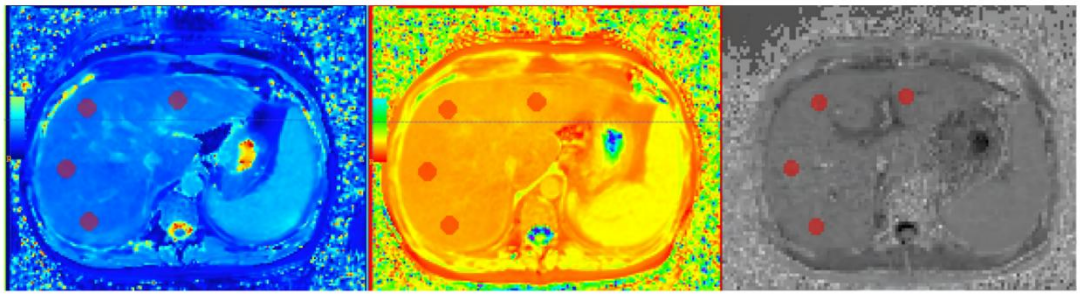


Figure 1(a-c). T1 mapping and vMRE images. (a) Pre-contrast T1 mapping (T1-pre). (b) T1 mapping acquired 20 minutes after contrast administration (T1-20min). (c) Virtual magnetic resonance elastography (vMRE).

2.5 Post-processing of vMRE and Acquisition of Stiffness Values

vMRE stiffness was quantified offline using MATLAB R2021a (MathWorks, Natick, MA, USA). According to a previous study [5], vMRE images can be obtained using only two b-values, typically 200 and 1500 s/mm², from which the shifted apparent diffusion coefficient (sADC) is calculated as: sADC = ln(S200/S1500) / (1500-200), where sADC is in mm²/s, and S200 and S1500 are the signal intensities at b = 200 and 1500 s/mm², respectively. ROIs for vMRE were placed on the same liver segments as T1 mapping ROIs, avoiding visible intrahepatic vessels and focal lesions (**Error! Reference source not found.**c). Stiffness was then calculated using the formula μDiff = α × sADC + β, where μDiff is the diffusion-based shear modulus reflecting tissue stiffness (kPa), sADC is the shifted ADC, and α and β were set to −9.8 ± 0.8 and 14.0 ± 0.9, respectively [6].vMRE values are derived from DWI signal fitting and are not directly equivalent to MRE-derived shear modulus; the kPa values reported here should be interpreted as protocol-specific estimates.

2.6 ICG clearance test

Patients fasted for 6–8 hours and emptied their bladder and bowel. Height, weight, and hemoglobin were entered into the analyzer (Nihon Kohden). ICG (0.5 mg/kg) was injected via a cubital vein catheter. After 15 minutes of supine rest, ICG-R15 was automatically calculated as the 15-minute retention rate.

2.7 Serological Parameters and FIB-4 Stratification

FIB-4 is a clinical tool used for liver fibrosis risk stratification. It is recommended by major hepatology societies, including the American Association for the Study of Liver Diseases (AASLD) [7], the European Association for the Study of the Liver (EASL), and the American Gastroenterological Association (AGA), as a first-line index for initial fibrosis risk stratification. The score is generated based on age ,AST (U/L), ALT (U/L), and PLT ($\times 10^9$/L), using the following formula: FIB-4 = (age × AST) / (PLT $\times$ALT$^{1/2}$). The FIB-4 cutoffs were: low-risk group < 1.45, intermediate-risk group 1.45–3.25, and high-risk group> 3.25.

2.8 Statistical Analysis

Statistical analysis was performed using SPSS 27.0 (IBM, Armonk, NY, USA). Normality was assessed by the Shapiro–Wilk test. Normally distributed data were presented as mean ± SD. Non-normally distributed data were presented as median (IQR). Group comparisons used one-way ANOVA or the Kruskal–Wallis test with Bonferroni correction. Categorical variables were compared using the χ^2 test. Correlations were evaluated by Spearman's rank correlation. Correlation strength was defined as: weak ($|r|<0.3$), moderate ($0.3\leq|r|<0.6$), strong ($0.6\leq|r|<0.8$), and very strong ($|r|\geq0.8$). ROC curves were constructed for the high-risk FIB-4 group. FIB-4 risk stratification is not a histopathological gold standard. The ROC analysis was exploratory. Multiple linear regression (Enter method) was performed

with vMRE as the dependent variable and FIB-4, age, and sex as independent variables. Collinearity (VIF) and residual independence (Durbin–Watson) were assessed. This regression was exploratory. It aimed to explore whether FIB-4 risk strata and other clinical factors are associated with vMRE measurements. The statistical objectives were: (1) to compare vMRE, T1-pre, T1-20min, ΔT1%, and ICG-R15 across FIB-4 risk strata; (2) to assess their correlation with FIB-4 risk stratification; and (3) to explore their ability to identify the high-risk group and factors associated with vMRE. All tests were two-sided, with $P<0.05$ considered statistically significant.

1321. RESULTS

A total of 86 patients (69 males and 17 females) were ultimately enrolled. Based on FIB-4 scores, patients were divided into low, intermediate, and high fibrosis risk groups . Baseline characteristics of each group are shown in **Error! Not a valid bookmark self-reference.**.

Table 1.Baseline characteristics of patients

Variable	Low-risk group (n=11)	Intermediate-risk group (n=30)	High-risk group (n=45)	Test statistic	*P*
Age (years)	50.0±11.3	56.9±8.3	57.02±10.2	$F(2,83) = 2.473$	0.090
Sex (M/F)	6/5	26/4	37/8	$\chi^2(2) = 5.472$	0.065
AST (U/L)	22（18-35）	31（22.5-38.0）	57（35.5-88.5）	$H(2) = 27.005$)	<0.001***
ALT (U/L)	22（12-38）	33（19.3-47.5）	45（20.5-75）	$H(2) = 6.515$	0.038*
PLT(×10^9/L)	260（189-327）	166（142-193.5）	112（71.5-137）	$H(2) = 37.241$	<0.001***

Data were expressed as mean ± SD or median (interquantile). Ast, aspartate aminotransferase; Alt,

alanine aminotransferase; Plt, platelet count; M, male; F, female; *p<0.05, **p<0.01, ***p<0.001

3.1 Comparison of parameters across different fibrosis risk groups

The distributions of vMRE, T1-pre, T1-20min, ΔT1%, and ICG-R15 across the low-, intermediate-, and high-risk groups, along with the results of intergroup comparisons, are presented inTable 2, and the distribution trends are visually illustrated by boxplots (Figure 2). T1-pre was normally distributed, with significant differences among the three groups (P<0.001). Post-hoc comparisons showed a significant difference between the intermediate- and high-risk groups (P<0.001), but not between the low- and intermediate-risk groups (P=0.916) or between the low- and high-risk groups (P=0.067). vMRE, T1-20min, ΔT1%, and ICG-R15 were non-normally distributed, and all four parameters showed significant differences across FIB-4 risk strata (P<0.001). Post-hoc pairwise comparisons revealed that vMRE differed significantly between any two groups (all P<0.001). For T1-20min, ΔT1%, and ICG-R15, significant differences were observed only in comparisons involving the high-risk group (all P<0.001), with no significant differences between the low- and intermediate-risk groups.

Table 2.Comparison of MRI and ICG parameters among FIB-4 risk groups

Variable	Low-risk (n=11)	Intermediate-risk (n=30)	High-risk (n=45)	*P*	Low vs Int	Low vs Hign	Int vs Hign
vMRE (kPa)	5.4(4.85–5.99)	6.3(6.06–6.47)	6.7(6.42–7.10)	*H*(2)=34.058 *P*<0.001***	*Z*=-3.766 *P*<0.001***	*Z*=-4.650 *P*<0.001***	*Z*=-4.012 *P*<0.001***

				F(2,83)=8.80	MD=10.648	MD=-51.415	MD=-68.063
T1-pre (ms)	618.8±52.6	608.2±68.9	676.2±83.6				
				P<0.001***	*P*=0.916	*P*=0.067	*P*<0.001***
	128.5	147.7	215.5(175.99–	*H*(2)=22.805	Z=-1.148	Z=-3.867	Z=-3.764
T1-20min (ms)							
	(102.11–151.86)	(110.32–208.89)	301.75)	*P*<0.001***	*P*=0.251	*P*<0.001***	*P*<0.001***
	-0.77(-0.830 to -	-0.75(-0.800 to -	-0.67(-0.725 to	H(2)=20.576	Z=-1.557	Z=-3.724	Z=-3.436
ΔT1%							
	0.750)	0.693)	-0.515)	*P*<0.001***	*P*=0.115	*P*<0.001***	*P*<0.001***
			11.9(6.30–	*H*(2)=19.690	Z=-0.765	Z=-3.342	Z=-3.721
ICG-R15 (%)	3.2（2.4-6.5）	4.9(2.58–7.68)					
			23.75)	*P*<0.001***	*P*=0.444	*P*<0.001***	*P*<0.001***

153 Data are expressed as mean ± SD or median (IQR) unless otherwise specified. vMRE, virtual magnetic
154 resonance elastography; T1-pre, pre-contrast T1 relaxation time; T1-20min, T1 relaxation time at 20
155 minutes post-contrast; ΔT1%, T1 change rate, calculated as (T1-20min − T1-pre) / T1-pre × 100%; ICG-
156 R15, indocyanine green retention rate at 15 minutes. **P*<0.05, ***P*<0.01, ****P*<0.001.

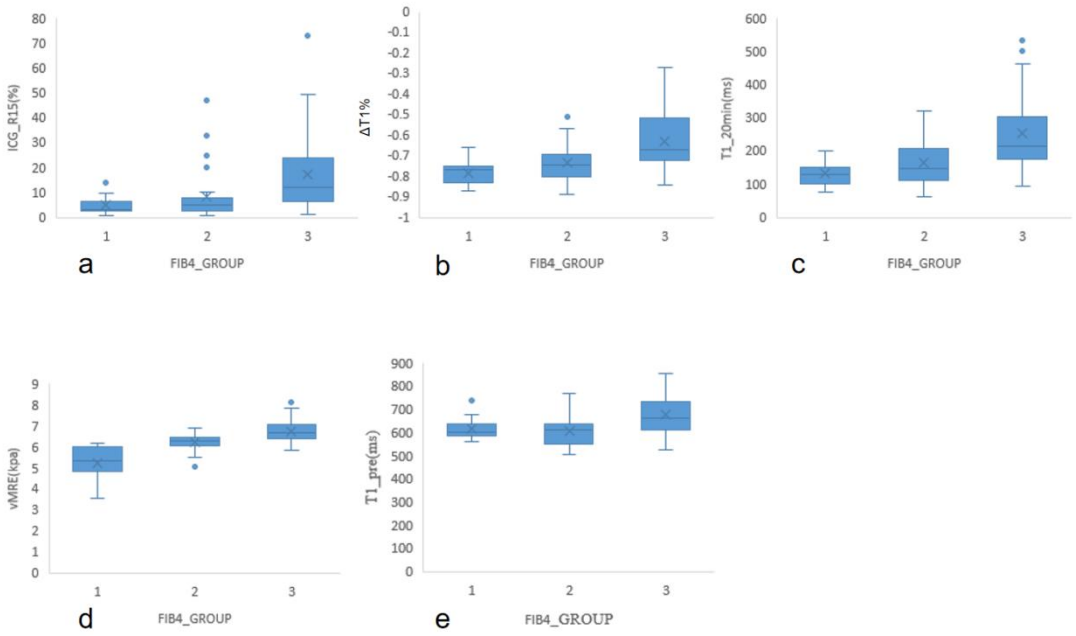


Figure 2（a-e）.Boxplots of vMRE, T1-pre, T1-20min, ΔT1%, and ICG-R15 among FIB-4 risk groups (a) ICG-R15, (b) ΔT1%, (c) T1-20min, (d) vMRE, and (e)T1-pre , In each box, the central line indicates the median, the box limits denote the interquartile range (IQR), and the whiskers extend to the range (minimum to maximum).

3.2 Correlation analysis between parameters and FIB-4

The results of Spearman's rank correlation analysis are presented in Table 3. vMRE showed weak positive correlations with T1-20min (r=0.27, *P*=0.012), ΔT1% (r=0.29, *P*<0.001), and ICG-R15 (r=0.31, *P*<0.001), and a moderate positive correlation with FIB-4 (r=0.49). T1-20min was very strongly correlated with ΔT1% (r=0.98, *P*<0.001). ICG-R15 was strongly correlated with FIB-4 (r=0.63).

Table 3. Spearman correlation matrix and correlations with FIB-4

Variable	vMRE (kPa)	T1-pre (ms)	T1-20min (ms)	ΔT1%	ICG-R15 (%)	Correlation with FIB-4
vMRE (kPa)	1	—	—	—	—	0.49(0.31-0.63)

	0.05(-0.16-0.26)					
T1-pre (ms)		1	—	—	—	0.43(0.24-0.59)
	$p = 0.666$					
	0.27(0.07-0.45)	0.63(0.48-0.74)				
T1-20min (ms)			1	—	—	0.61(0.46-0.73)
	$p = 0.012$*	$p < 0.001$***				
	0.29(0.09-0.47)	0.47(0.29-0.62)	0.98(0.97-0.99)			
ΔT1%				1	1	0.59(0.43-0.71)
	$p < 0.001$***	$p < 0.001$***	$p < 0.001$***			
ICG-R15	0.31(0.11-0.48)	0.44(0.25-0.59)	0.70(0.57-0.79)	0.69(0.56-0.79)		
					1	0.63(0.48-0.74)
(%)	$p < 0.001$***	$p < 0.001$***	$p < 0.001$***	$p < 0.001$***		

Data are presented as Spearman correlation coefficient r (95% CI). r, Spearman rank correlation coefficient; 1, self-correlation; —, omitted due to symmetry; 95% CI, 95% confidence interval (calculated using Fisher's z-transformation); *P<0.05, **P<0.01, ***P<0.001.

3.3 ROC curve analysis

The ROC curves of each parameter for identifying the high-risk group are shown in Error! Unknown switch argument.**,** and the detailed analysis results are presented in Table 4. With FIB-4 risk stratification as the reference, vMRE yielded the highest AUC (0.823), with an optimal cut-off value of 6.55 kPa, yielding a sensitivity of 68.9% and a specificity of 87.8%. DeLong's test revealed that the AUC of vMRE was significantly larger than that of T1-pre (P=0.032), whereas no significant differences were observed compared with T1-20min, ΔT1%, or ICG-R15.

Table 4. ROC curve analysis for indentifying the high-risk FIB-4 group

Variable	AUC (95% CI)	*P*	Optimal cut-off value	Sensitivity	Specificity
vMRE (kPa)	0.823(0.735–0.912)	< 0.001***	6.55	68.9%	87.8%
T1-pre (ms)	0.734(0.628–0.840)	< 0.001***	642.30	66.7%	78.0%
T1-20min (ms)	0.790(0.695–0.886)	< 0.001***	175.27	77.8%	70.7%
ΔT1%	0.770(0.670–0.870)	< 0.001***	0.73	75.6%	73.2%
ICG-R15 (%)	0.774(0.672–0.877)	< 0.001***	9.15	68.9%	80.5%

AUC, area under the receiver operating characteristic curve; CI, confidence interval. Optimal cut-off values were selected based on the maximum Youden index. **P*<0.05, ***P*<0.01, ****P*<0.001.

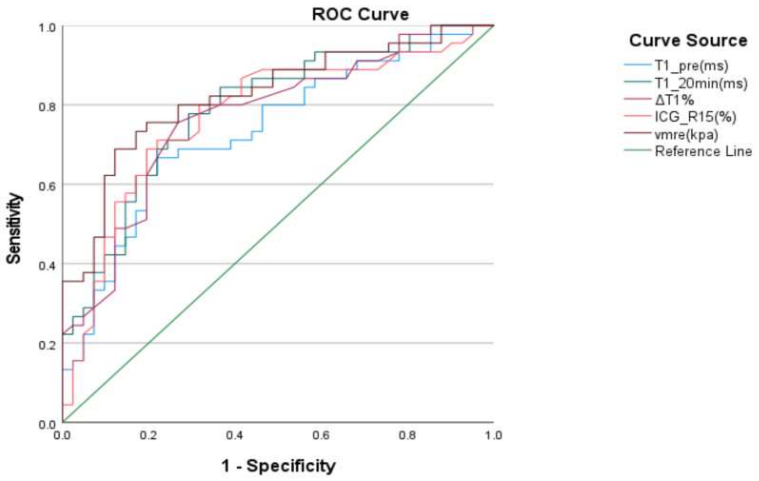


Figure 3.ROC curves of vMRE, T1-pre, T1-20min, ΔT1%, and ICG-R15 for identifying the high-risk group (FIB-4 > 3.25). The curves represent vMRE (kPa), T1-pre (ms), T1-20min (ms), ΔT1%, and ICG-R15 (%), respectively. The diagonal dashed line is the reference line (AUC = 0.5, indicating no discriminative ability). Curves closer to the upper-left corner indicate better discriminative performance.

3.4 Multiple linear regression analysis

A multiple linear regression model was constructed using the Enter method, with vMRE as the dependent variable and FIB-4, age, and sex as independent variables. This regression was exploratory and aimed to identify factors associated with vMRE measurements, rather than to establish a predictive model for fibrosis. The results are presented in The overall model was statistically significant ($F(3, 82)=9.175$, $P<0.001$), with an adjusted R^2 of 0.224. FIB-4 was independently associated with vMRE (B=0.088, 95% CI: 0.050–0.124, $P<0.001$; β=0.447). Sex was also independently associated with vMRE (females showed lower values by 0.417 kPa, 95% CI: 0.059–0.776, $P=0.023$), whereas age showed no significant association ($P=0.290$). Multicollinearity was not detected (VIF close to 1 for all variables), and the Durbin-Watson statistic (1.822) indicated satisfactory residual independence.

Table 5. The overall model was statistically significant ($F(3, 82)=9.175$, $P<0.001$), with an adjusted R^2 of 0.224. FIB-4 was independently associated with vMRE (B=0.088, 95% CI: 0.050–0.124, $P<0.001$; β=0.447). Sex was also independently associated with vMRE (females showed lower values by 0.417 kPa, 95% CI: 0.059–0.776, $P=0.023$), whereas age showed no significant association ($P=0.290$). Multicollinearity was not detected (VIF close to 1 for all variables), and the Durbin-Watson statistic (1.822) indicated satisfactory residual independence.

Table 5. Multiple linear regression analysis of factors influencing vMRE

Independent variable	Unstandardized coefficient B (95% CI)	Standard error (SE)	Standardized coefficient (Beta)	t-value	*P*	VIF
Constant	5.259 (4.402–6.115)	0.430		12.215	<0.001***	—
FIB-4	0.088 (0.050–0.127)	0.019	0.447	4.621	<0.001***	1.027

Age	0.008 (-0.007–0.022)	0.007	0.103	1.064	0.290	1.018
Sex (F=0, M=1)	0.417(0.059–0.776)	0.180	0.224	2.318	0.023	1.018

Dependent variable: vMRE (kPa). VIF, variance inflation factor; all VIF < 2, indicating no significant multicollinearity. Values in parentheses for B are 95% confidence intervals. Sex coded as F=0, M=1. **P*<0.05, ***P*<0.01, ****P*<0.001.

2. DISCUSSION

Chronic liver injury activates hepatic stellate cells and promotes extracellular matrix (ECM) deposition [8], resulting in progressive liver stiffness, which has a direct pathophysiological correlation with fibrosis progression [9]. As a virtual elastography technique that does not require an external driver, vMRE sensitively reflected changes in liver stiffness in this study. Its values showed a stepwise increase across FIB-4 risk groups (5.4 kPa → 6.3 kPa → 6.7 kPa), with statistically significant differences between any two groups. This gradient correlation, consistent with fibrosis stage progression, supports the core mechanism by which progressive ECM deposition remodels tissue mechanical properties through altering water diffusion characteristics[10], indicating that vMRE effectively captures biomechanical microenvironmental changes during liver fibrosis progression. For identifying the high-risk group, vMRE yielded an AUC of 0.823 for identifying the high-risk group, consistent with findings from studies that used histopathology as the reference standard. A meta-analysis by Liang et al. [11] reported an AUC of 0.94 for magnetic resonance elastography (MRE) in diagnosing cirrhosis. Although the AUC of vMRE in our study was slightly lower than this pooled estimate, it remained within the same order of magnitude. Yang et al. [12] also confirmed in 111 patients with chronic liver disease that the DWI-based vMRE (denoted as the diffusion-based shear modulus, μDiff) achieved an AUC of 0.89 for

diagnosing advanced fibrosis and showed a moderate positive correlation with fibrosis stage (rho = 0.54, $P < 0.001$). However, Yang et al. reported that 2D-SWE outperformed vMRE, and Onar et al. [13]found that vMRE achieved an AUC of only 0.45–0.76 in a biopsy-controlled cohort, with better performance in the HBV subgroup. These findings suggest that vMRE performance may vary by etiology and fibrosis stage. Furthermore, a study by Kromrey et al. [14] using conventional MRE as a reference demonstrated that μDiff was in good agreement with the MRE-derived shear modulus (μMRE), with $r^2 = 0.81$ and a mean difference of −0.02 ± 0.88 kPa. Our findings further validate the clinical utility of vMRE for assessing background liver fibrosis in FLL patients, suggesting that vMRE may provide supplementary information when MRE is not available.

The key finding of this study was that vMRE showed statistically significant differences between the low- and intermediate-risk groups, whereas T1-pre, T1-20min, and ΔT1% did not differ significantly at this stage. These findings suggest that functional changes at earlier stages may be masked by hepatic compensatory reserve, while vMRE can detect structural changes at this stage. These findings warrant validation in larger cohorts. The earlier detection of structural parameters may be explained as follows. In the early stages of fibrosis, abnormal extracellular matrix (ECM) deposition and microstructural reorganization, including collagen cross-linking, can lead to a progressive increase in tissue stiffness [15,16]. Since vMRE reflects changes in stiffness, it was able to detect intergroup differences at an early stage. Moreover, the elevation of tissue stiffness itself can drive hepatic stellate cell activation through mechanical signaling pathways, forming a mechanobiological positive feedback loop that sustains and amplifies collagen secretion [17,18]. This self-accelerating mechanism suggests that once structural alterations occur, they rapidly widen the gap between structural and functional parameters. In contrast, functional abnormalities do not become apparent until the buffering capacity of

hepatic reserve is exceeded [19]. he lag mechanisms vary across different functional parameters. For T1-pre, the delay is attributable to a threshold effect. Meng et al. [20]demonstrated that T1 signals are confounded by metabolic factors such as fat and iron, rather than reflecting fibrosis alone. Furthermore, von Ulmenstein et al. [21] showed that T1 mapping gains discriminative power only when fibrosis is accompanied by substantial histological remodeling, suggesting that differences can be detected only when the disease burden surpasses a certain critical threshold. The lag mechanisms for T1-20min and ΔT1% differ from that of T1-pre. Although organic anion transporting polypeptide (OATP) transporter function is already impaired in the early stages of fibrosis [22,23], compensatory hyperplasia of residual hepatocytes can maintain overall uptake function, such that significant imaging differences for ΔT1% only emerge at moderate-to-advanced fibrotic stages. The absence of corresponding significant changes in ΔT1% in this study is likely attributable to compensatory hyperplasia of residual hepatocytes and upregulation of per-cell uptake capacity. If the aforementioned temporal pattern is validated in larger cohorts, vMRE holds promise as a preferred non-invasive tool for preoperative assessment of low-to-intermediate fibrosis in FLL patients. Its integration into routine MRI protocols could provide quantitative mechanical information on background liver fibrosis without increasing scan time.

At the functional assessment level, ΔT1% showed a very strong positive correlation with T1-20min, which is consistent with their mathematical homology. As a relative value, ΔT1% eliminates individual baseline variability through self-correction, thereby offering better comparability than T1-20min [24]. In this study, ΔT1% showed a strong correlation with ICG-R15 and yielded an AUC of 0.770 for identifying the high-risk group. Ai et al. [25] reported pooled correlation coefficients between ICG-R15 and several functional parameters, including RLE, rrT1, LSR, and LMR, and our results are directionally consistent with their findings. Notably, the correlation coefficient (ρ) observed in our study

was higher than their pooled estimates, which is likely attributable to our use of a calculation method based on the rate of change in T1 relaxation time. Xu et al. [26]further demonstrated in a rat model that ΔT1 (T1 reduction rate) was significantly correlated with ICG-R15 (r = 0.685, P = 0.029), providing a preclinical evidence chain that supports the findings of our human study. Our findings are consistent with previous reports and further support the value of ΔT1% as a non-invasive biomarker for liver function reserve. Compared with ICG-R15, ΔT1% can be obtained simultaneously during routine Gd-EOB-DTPA-enhanced MRI, making it particularly suitable for patients who cannot tolerate ICG testing or require repeated assessments of liver function reserve [27,28].

In this study, a regression model was constructed with vMRE as the dependent variable and FIB-4, age, and sex as independent variables. The aim was to assess whether the fibrosis risk represented by FIB-4 was independently associated with vMRE stiffness. Our results showed that FIB-4 was independently associated with vMRE (B=0.088, P<0.001). This finding is consistent with the conclusion of Besa et al. [29], who confirmed that both MR stiffness and FIB-4 were independently associated with fibrosis stage, with superior performance when combined, using histopathology as the reference standard. Together, these two studies suggest that the independent association between FIB-4 and MRI-derived stiffness parameters is reproducible across different elastography techniques.

In terms of gender, male vMRE was 0.417 kPa higher than female vMRE. This difference may be related to the mechanism by which 17α-estradiol inhibits hepatic stellate cell activation through estrogen receptorβ [30]. However, MRE studies in healthy populations have not demonstrated an independent effect of sex on liver stiffness [9,31], suggesting that this difference may only manifest under pathological conditions and should therefore be interpreted with caution.Age showed no independent correlation with vMRE. Liang et al. [28], an individual patient data meta-analysis, concluded that age

was not a significant confounder for MRE-based diagnosis, which is fully consistent with this finding. The adjusted R^2 of this model was 0.224, indicating that sex, age, and FIB-4 explained about 22% of the variance in vMRE stiffness. However, this low R^2 should not be interpreted as a model flaw, as stiffness measurements are also influenced by inflammation, hemodynamics, and steatosis [31–33]. These factors were not included in the current model, which may partly account for the low R^2. In addition, patients with markedly elevated ALT/AST were excluded to minimize interference from acute liver injury, and the heterogeneous etiologies of FLL in this cohort further limit the explanatory power of FIB-4. Despite the limited R^2, FIB-4 remained independently associated with vMRE, suggesting that a fibrosis-related signal is indeed present in vMRE. Future prospective studies with more homogeneous etiologies and inclusion of covariates such as inflammatory and metabolic factors will help further decompose the sources of variance in vMRE stiffness.

5. CONCLUSION

In this study, vMRE showed significant differences across all FIB-4 risk strata, whereas gadoxetate-enhanced T1 parameters showed differences only in some strata. These distinct patterns suggest that the two techniques may capture different aspects of liver pathology. The combination of vMRE and ΔT1% may provide complementary information, but its clinical value requires further validation.

6. LIMITATIONS

This study has several limitations. First, FIB-4 risk stratification is not a histopathological gold standard, and its strata do not represent true fibrosis stages. Second, vMRE values are derived from DWI signal fitting and are not directly comparable to MRE-derived shear modulus thresholds. Third, ALT was retrospectively collected and could not be controlled. Fourth, the sample size was limited. Fifth, the lack

of histopathological reference requires prospective validation.

REFERENCES

1. Frenette C, Mendiratta-Lala M, Salgia R, Wong RJ, Sauer BG, Pillai A. ACG Clinical Guideline: Focal Liver Lesions. Am J Gastroenterol. 2024;119:1235–71. https://doi.org/10.14309/ajg.0000000000002857

2. Kalil JA, Deschenes M, Perrier H, Zlotnik O, Metrakos P. Navigating Complex Challenges: Preoperative Assessment and Surgical Strategies for Liver Resection in Patients with Fibrosis or Cirrhosis. Biomedicines. 2024;12:1264. https://doi.org/10.3390/biomedicines12061264

3. Nevola R, Ruocco R, Criscuolo L, Villani A, Alfano M, Beccia D, et al. Predictors of early and late hepatocellular carcinoma recurrence. World J Gastroenterol. 2023;29:1243–60. https://doi.org/10.3748/wjg.v29.i8.1243

4. Lee J, Vali Y, Boursier J, Spijker R, Anstee QM, Bossuyt PM, et al. Prognostic accuracy of FIB-4, NAFLD fibrosis score and APRI for NAFLD-related events: A systematic review. Liver Int. 2021;41:261–70. https://doi.org/10.1111/liv.14669

5. Zou Y, Chen J, Liao J. Diagnostic Evaluation of Liver Fibrosis using B1-Corrected T1 Mapping and DWI-Based Virtual Elastography. Curr Med Imaging. 2025;21:e15734056401119. https://doi.org/10.2174/0115734056401119250908130930

6. Aunan-Diop JS, Andersen MCS, Friismose AI, Halle B, Pedersen CB, Mussmann B, et al. Virtual magnetic resonance elastography predicts the intraoperative consistency of meningiomas. J Neuroradiol. 2023;50:396–401. https://doi.org/10.1016/j.neurad.2022.10.006

7. Rinella ME, Neuschwander-Tetri BA, Siddiqui MS, Abdelmalek MF, Caldwell S, Barb D, et

al. AASLD Practice Guidance on the clinical assessment and management of nonalcoholic fatty liver disease. Hepatology. 2023;77:1797–835. https://doi.org/10.1097/HEP.0000000000000323

8. Zhao Y-Q, Deng X-W, Xu G-Q, Lin J, Lu H-Z, Chen J. Mechanical homeostasis imbalance in hepatic stellate cells activation and hepatic fibrosis. Front Mol Biosci. 2023;10:1183808. https://doi.org/10.3389/fmolb.2023.1183808

9. Obrzut M, Atamaniuk V, Obrzut B, Ehman R, Cholewa M, Rzucidło M, et al. Normative values for magnetic resonance elastography-based liver stiffness in a healthy population. Pol Arch Intern Med. 2019;129:785–91. https://doi.org/10.20452/pamw.4456

10. Huang X. Optimized DWI-based virtual MR elastography for diagnosis and therapeutic monitoring of focal liver lesions. Eur J Radiol. 2025;191:112285. https://doi.org/10.1016/j.ejrad.2025.112285

11. Liang Y, Li D. Magnetic resonance elastography in staging liver fibrosis in non-alcoholic fatty liver disease: a pooled analysis of the diagnostic accuracy. BMC Gastroenterol. 2020;20:89. https://doi.org/10.1186/s12876-020-01234-x

12. Yang L, Zhou G, Liu L, Rao S, Wang W, Jin K, et al. Assessing liver fibrosis in chronic liver disease: Comparison of diffusion-weighted MR elastography and two-dimensional shear-wave elastography using histopathologic assessment as the reference standard. Ann Hepatol. 2025;30:101743. https://doi.org/10.1016/j.aohep.2024.101743

13. Onar MA, Nural MS, Deveci A, Meydan BC. Evaluation of liver fibrosis using diffusion-weighted virtual magnetic resonance elastography and ultrasound elastography. Abdom Radi

ol. 2025;51:3–13. https://doi.org/10.1007/s00261-025-05043-2

14. Kromrey M-L, Le Bihan D, Ichikawa S, Motosugi U. Diffusion-weighted MRI-based Virtual Elastography for the Assessment of Liver Fibrosis. Radiology. 2020;295:127–35. https://doi.org/10.1148/radiol.2020191498

15. Zhang W, Zhang N, Wu W, Li H, You H, Chen W. Atlas of mildly and highly insoluble matrisome driving liver fibrosis. Front Pharmacol. 2024;15:1435359. https://doi.org/10.3389/fphar.2024.1435359

16. Yue W, Zhang H, Gao Y, Ding J, Xue R, Dong C, et al. Procollagen-lysine 2-oxoglutarate 5-dioxygenase 2 promotes collagen cross-linking and ECM stiffening to induce liver fibrosis. Biochim Biophys Acta Mol Basis Dis. 2024;1870:167205. https://doi.org/10.1016/j.bbadis.2024.167205

17. Min K, Karuppannan SK, Tae G. The impact of matrix stiffness on hepatic cell function, liver fibrosis, and hepatocellular carcinoma-Based on quantitative data. Biophys Rev. 2024;5:021306. https://doi.org/10.1063/5.0197875

18. Kostallari E, Wei B, Sicard D, Li J, Cooper SA, Gao J, et al. Stiffness is associated with hepatic stellate cell heterogeneity during liver fibrosis. Am J Physiol Gastrointest Liver Physiol. 2022;322:G234–46. https://doi.org/10.1152/ajpgi.00254.2021

19. Qiu T, Yang J, Peng C, Xiang H, Huang L, Ling W, et al. Diagnosis of liver fibrosis and liver function reserve through non-invasive multispectral photoacoustic imaging. Photoacoustics. 2023;33:100562. https://doi.org/10.1016/j.pacs.2023.100562

20. Meng Z, Deng S, Zhu X, Guo Y, Su B, Cao J, et al. T2-MAP outperforms native T1-MA

P for staging liver fibrosis independent of steatosis and iron overload: A dual-cohort causa
l validation study. Eur J Radiol. 2026;203:113015. https://doi.org/10.1016/j.ejrad.2026.11301
5

21. Von Ulmenstein S, Bogdanovic S, Honcharova-Biletska H, Blümel S, Deibel AR, Segna D,
et al. Assessment of hepatic fibrosis and inflammation with look-locker T1 mapping and
magnetic resonance elastography with histopathology as reference standard. Abdom Radiol.
2022;47:3746–57. https://doi.org/10.1007/s00261-022-03647-6

22. Sheng RF, Wang HQ, Yang L, Jin KP, Xie YH, Fu CX, et al. Assessment of liver fibrosi
s using T1 mapping on Gd-EOB-DTPA-enhanced magnetic resonance. Dig Liver Dis. 2017
;49:789–95. https://doi.org/10.1016/j.dld.2017.02.006

23. Pippa LF, Vieira CP, Caris JA, Rocha A, Marques MP, Garcia CP, et al. Effect of Chronic
Hepatitis C on the Activity of the Membrane Transporters P-gp and OATP1B1/BCRP on
Patients With Different Stages of Hepatic Fibrosis. Clin Pharmacol Ther. 2023;114:173–81.
https://doi.org/10.1002/cpt.2908

24. Wang Q, Kesen S, Liljeroth M, Nilsson H, Zhao Y, Sparrelid E, et al. Quantitative evaluat
ion of liver function with gadoxetic acid enhanced MRI: Comparison among signal intensit
y-, T1-relaxometry-, and dynamic-hepatocyte-specific-contrast-enhanced MRI- derived param
eters. Scand J Gastroenterol. 2022;57:705–12. https://doi.org/10.1080/00365521.2022.2032321

25. Ai X, Wang H, Yang Y, Feng Y, Xie X, Zhao X, et al. Four indices on Gd-EOB-DTPA-e
nhanced MRI can estimate liver functional reserve compared to ICG-R15: A systematic re
view and meta-analysis. Clin Imaging. 2023;102:1–8. https://doi.org/10.1016/j.clinimag.2023.

06.018

26. Xu J, Wang X, Jin Z, Wang Q, You Y, Wang S, et al. Assessing Liver Function by T1 Maps on Gd-EOB-DTPA-Enhanced MRI for up to 50 Min in Rat Models of Liver Fibrosis: A Longer Hepatobiliary Time Period may Help. Chin Med Sci J. 2021;36:110–9. https://doi.org/10.24920/003794

27. Kim JE, Kim HO, Bae K, Choi DS, Nickel D. T1 mapping for liver function evaluation in gadoxetic acid–enhanced MR imaging: comparison of look-locker inversion recovery and B1 inhomogeneity–corrected variable flip angle method. Eur Radiol. 2019;29:3584–94. https://doi.org/10.1007/s00330-018-5947-4

28. Zhang G, Li M, Feng H, Ren Y, Jin X, Ke Q, et al. Hepatocyte uptake ratio derived from T1 mapping for quantitative assessment of liver fibrosis. Eur Radiol. 2026;36:1411–20. https://doi.org/10.1007/s00330-025-11842-4

29. Besa C, Wagner M, Lo G, Gordic S, Chatterji M, Kennedy P, et al. Detection of liver fibrosis using qualitative and quantitative MR elastography compared to liver surface nodularity measurement, gadoxetic acid uptake, and serum markers. J Magn Reson Imaging. 2018;47:1552–61. https://doi.org/10.1002/jmri.25911

30. Ali Mondal S, Sathiaseelan R, Mann SN, Kamal M, Luo W, Saccon TD, et al. 17α-estradiol, a lifespan-extending compound, attenuates liver fibrosis by modulating collagen turnover rates in male mice. Am J Physiol Endocrinol Metab. 2022;324:E120–34. https://doi.org/10.1152/ajpendo.00256.2022

31. Wei X, Qi S, Wei X, Qiu L, Du X, Liu Y, et al. Inflammation activity affects liver stiffn

ess measurement by magnetic resonance elastography in MASLD. Dig Liver Dis. 2024;56: 1715–20. https://doi.org/10.1016/j.dld.2024.04.031

32. Serai SD, Tsitsiou Y, Wilkins BJ, Ghosh A, Cahill AM, Biko DM, et al. MR elastography -based staging of liver fibrosis in Fontan procedure associated liver disease is confounded by effects of venous congestion. Clin Radiol. 2022;77:e776–82. https://doi.org/10.1016/j.crad .2022.06.016

33. Nakano C, Nishimura T, Tada T, Yoshida M, Takashima T, Aizawa N, et al. Severity of li ver fibrosis using shear wave elastography is influenced by hepatic necroinflammation in c hronic hepatitis patients, but not in cirrhotic patients. Hepatol Res. 2021;51:436–44. https:// doi.org/10.1111/hepr.13617

DECLARATIONS

Ethics approval and consent to participate: This retrospective study was approved by the Et hics Committee of The First People's Hospital of Yunnan Province (Approval No. KKHLL -LCYJ2026-477). It was conducted in accordance with the Declaration of Helsinki. The re quirement for informed consent was waived by the ethics committee due to the retrospecti ve and anonymized nature of the study.

Consent for publication: Not applicable.

Availability of data and materials: The datasets generated during and/or analyzed during the current study are available from the corresponding author on reasonable request.

Competing interests: The authors declare that they have no competing interests.

Funding: This research received no specific grant from any funding agency in the public, com

mercial, or not-for-profit sectors.

Authors' contributions: W.B. led the conception and design of the study, provided overall supervision, and finalized the manuscript. X.W.J. collected the clinical and imaging data, delineated the regions of interest (ROIs), performed the statistical analysis, and drafted the main manuscript text. W.L. provided methodological guidance and critically revised the manuscript for important intellectual content. Y.J. provided the virtual MR elastography technology and assisted in revising the figures and tables. X.C.Y. collected the clinical and imaging data and delineated the regions of interest (ROIs). All authors read and approved the final manuscript.

Acknowledgements: Not applicable.